Discontinuities in granular materials: Particle-level mechanisms

J. Carlos Santamarina and Hosung Shin

Georgia Institute of Technology, Atlanta, GA 30328

Abstract Discontinuous planes often develop in soils and affect the mechanical behavior (stiffness and strength) and transport properties of sediments (fluid migration and diffusion). The fundamental understanding of the development of discontinuities in soils must recognize their inherent granular nature and effective-stress dependent behavior. We use complementary experimental, analytical and numerical methods to study particle-scale mechanisms involved in contraction-driven shear failure due to mineral dissolution, desiccation cracks, and hydraulic fractures. We show that: (1) under zero-lateral strain conditions, particle-scale volume contraction causes a stress decrease from k_0-to-k_a so that shear strain localization can develop in sediments with post-peak strain softening response; (2) the development of desiccation cracks in fine grained sediments is determined by the invasion of the air-water interface membrane and ensuing changes in particle forces and displacements; (3) hydraulic fracture results from positive feedback between changes in pore size and the associated changes in particle-level capillary forces (immiscible fluids), seepage drag forces (miscible fluids) and skeletal forces. These particle-level mechanisms are compatible with the effective stress dependent frictional behavior of soils.

1. Introduction

Soils are granular materials; the granular skeleton and pore structure determine the mechanical and hydraulic properties of the soil mass. Strain localization planes in the granular mass can develop along sedimentation planes, or by changes in boundary and loading conditions that cause positive feedback and a runaway effect. These localizations have profound practical relevance because stability and deformation characteristics of geo-structures are often controlled by the presence of discontinuities that act as either weak zones or preferential paths for gas or fluid migration.

The development of discontinuities in granular materials has attracted much research attention, and various modes of failure have been identified, including open, closed, and shear discontinuities. Specific examples include shear bands, desiccation cracks, polygonal fault systems, ice lenses, hydraulic fractures, and grouting-induced fractures.

In this article we summarize a fundamental particle and pore scale understanding of localization mechanisms associated to mineral dissolution, desiccation cracks and hydraulic fracture. The complete study is documented in Shin (2009) and in references by the authors listed herein.

2. Mineral dissolution and shear strain localization

Shear failure in sediments is generally linked with active boundary conditions, such as those imposed by tectonic stresses. Under conditions of no lateral strain, and in the absence of tectonic stress, soil mechanic theories predict a simple one-dimensional compaction in which sediment particles displace vertically without shear failure during fluid pressure diffusion. Conflicting with this theory, shear failure planes are often found in sediments that formed under near horizontal burial conditions in zones with no tectonic activity.

Various thermo-chemo-hydro-mechanical coupling mechanisms were hypothesized to explain the development of these discontinuities. At present, mineral dissolution appears as the most plausible triggering mechanisms. We used experimental, analytical and numerical methods to explore the evolution of internal stresses, conditions for localization and the ensuing deformation field.

Evolution of internal stresses

Experimental results were obtained using a soft oedometer filled with a granular mixture of salt and glass beads saturated with brine. After loading, the pore fluid concentration was decreased gradually to dissolve the salt grains. The ratio between horizontal-to-vertical effective stress decreased from the initial value $k_0 \approx 1-\sin\phi$ (as in Jaky 1944) to a value similar to $k_a=\tan^2(45-\phi/2)$ at the Coulomb failure condition (experimental details and results in Shin and Santamarina

2009a). If dissolution continued, the horizontal stress increased towards k_0 with episodic changes in k.

Similar results were obtained using discrete element simulations, by decreasing the particle diameter for a randomly selected set of particles (Fig. 1). While horizontal stress recovery often follows upon further dissolution, marked differences in fabric are observed between the pre and post-dissolution fabrics.

Both experimental and numerical results showed the increase in void ratio and the development of loose packing after dissociation; this observation may explain the response of some natural soils (e.g., those reported in Burland 1990).

We can conclude that grain mass loss due to mineral dissolution produces a pronounced horizontal stress drop under zero lateral strain conditions and the state of stress may reach the active shear failure k_a-condition.

Shear localization

Shear strain localization and the formation of shear bands reflect the development of energetically new beneficial deformation mechanism whereby less energy is required to deform along a few planes rather than in the homogeneous deformation of the whole sediment. Mathematically, shear bands form when the strain hardening $h = \partial\sigma_d / \partial\gamma_{pl}$ exceeds a critical value h_{cr} (where σ_d is the deviatoric

stress and γ_{pl} is the plastic shear strain). The values of h_{cr} depend on material strength parameters and loading path (Rudnicki and Rice 1975). In the case of Drucker-Prager model with shear hardening, h_{cr} becomes (Perrin and Leblond 1993, Lade 2002)

$$\frac{h_{cr}}{G} = \frac{1+\nu}{9(1-\nu)}(\beta-\mu)^2 - \frac{1}{2}(1+\nu)\left[-N+\frac{1}{3}(\beta+\mu)\right]^2 \qquad (1)$$

where $\mu = \tan(\phi)$ and $\beta = \tan(\psi)$ capture the peak friction angle ϕ and the angle of dilation ψ. Stress anisotropy is represented the parameter $N = \sqrt{2}\sigma_2' / \sqrt{\sigma_1'^2 + \sigma_2'^2 + \sigma_3'^2}$.

In sediments that have experienced particle-level volume contraction, the stress in the vertical direction is the maximum principal stress and the two horizontal stresses are of the same magnitude. For this stress condition, shear faulting occurs in the strain softening regime in homogenous media; therefore, the formation of shear faults associated with volume contraction will take place in materials that exhibit post-peak strength softening.

A complex pattern of strain localization is anticipated because there is no preferred direction for shear planes (Desrues and Viggiani 2004). Polygonal faults emerge as a kinematically admissible fault morphology, as observed in the field (Cartwright and Dewhurst 1998).

To gain further insight into the potential development of shear strain localization during particle-level contraction, we conducted finite element simulations of a medium subjected to constant vertical stress under zero lateral strain boundary conditions using a Drucker-Prager frictional model with non-associated flow rule (details in Shin et al. 2008). The nucleation of localization was facilitated by creating a correlated random field for volume contraction. Results show diffused strain localization in perfectly plastic media $\phi_{res}= \phi_p$ (Fig. 2-a) and marked shear strain localization when the medium was modeled with post-peak strength softening $\phi_{res}<\phi_p$ (Fig. 2-b).

Deformation Field

The regions surrounding individual polygonal faults show evidence of local strain accumulations that closely match theoretically predicted near-field strains for blind normal faults (Barnett et al. 1987). Tectonic normal faults are widely considered to follow a simple scaling relationship between maximum displacement and maximum dimension (Cowie and Scholz 1992, Schultz et al. 2006). We collected data for maximum throw δ versus fault height H for 629 polygonal faults: all measurements are bound within $\delta/H=0.045\pm0.016$ (Shin et al. 2009). These are surprisingly large displacements for

systems that have not experienced extension in their basal planes, and the δ/H values are much larger than for most tectonic normal faults (as compared to trends in Cowie and Scholz 1992 at an effective stress σ′<40MPa).

Let's assume a shear plane at β=45°+ϕ/2 (Vermeer 1990). The stress redistribution after shear localization leads to a new horizontal stress ratio $k_r = \sigma'_{hr} / \sigma'_z$

$$k_r = \frac{\cos(\beta)\sin(\beta - \phi_r)}{\sin(\phi_r) + \cos(\beta)\sin(\beta - \phi_r)} \qquad (2)$$

The horizontal stress change from k_0 to k_r produces a contractive horizontal strain $\varepsilon_h = \Delta\sigma'_h / E$. We assume that the region where strains accumulate around the fault has a parabolic shape, and integrate horizontal strains to obtain the horizontal displacement u_h; finally, we compute the associated vertical displacement to satisfy compatibility, $u_z=u_h\tan\beta$. The maximum normalized throw δ/H predicted by this analysis is

$$\frac{\delta}{H} = \frac{(k_r - k_0)\tan(\beta)}{2} \frac{\sigma'_z}{E} \qquad (3)$$

which is a function of the horizontal stress change (k_r-k_0) and inversely proportional to sediment stiffness-to-stress ratio E/σ'_z.

Numerical simulations are conducted using a Drucker-Prager model where the Coulomb-type strength criterion is linearly proportional to

the effective confining stress, i.e., no cohesion. Predicted volumetric strains $\varepsilon_v \cdot q/E$ and normalized throw δ/H are shown in Fig. 3 (Note: the volumetric strain is normalized by the ratio between the vertical load q at the burial depth and the sediment stiffness E).

Numerical results (Fig. 3) and analytical predictions (Equation 3) match measured trends for very small values of stiffness $1.5<E/\sigma'_z<10$. (As a reference, standard values for sediments that have not experienced dissolution range from $E/\sigma' \sim 40$ at large strains to $E/\sigma' \sim 100$ for small strains - Santamarina, et al., 2001). Indeed, it can be shown that the normalized equivalent skeletal compressibility E_{eq}/σ' for sediments that experienced dissolution and exhibit high porosity before shear is

$$\frac{k_r - k_a}{\alpha} > \frac{E_{eq}}{\sigma'_z} > \frac{k_r - k_a}{\alpha + 0.3(1-\alpha)C_c/(1+e_0)} \qquad (4)$$

resulting in an estimate of $E_{eq}/\sigma' \approx$ 1.5-to-6 in sediments that went through α=10% dissolution. This low E_{eq}/σ' estimate is compatible with field observations and confirms the role of dissolution as a causal mechanism.

3. Desiccation cracks in saturated fine-grained soils

It is often assumed that soils crack when the tensile stress exceeds the soil tensile strength (Lachenbruch, 1962). However, this mecha-

nistic interpretation fails to recognize the inherent, cohesionless-yet-frictional effective stress dependent behavior of soils. Furthermore, assumptions such as zero effective stress at the crack tip may not necessarily reflect the underlying particle level mechanisms.

Fundamental Mechanism – Fine Grained Soils

A new hypothetical mechanism for desiccation crack initiation and growth is proposed herein, centered on the air-water interface membrane (Shin and Santamarina 2009b).

The sequence of events summarized in Fig. 4 has been identified from multiple experimental observations. (a) The water surface is above the sediment surface; water evaporates freely and the pore fluid pressure is positive everywhere inside the sediment. (b) Eventually, the water level reaches the sediment surface; at this instant, the pore fluid pressure on the surface is zero. (c) Further evaporation brings the air-water interface membrane against grain surfaces; the membrane resists invading the soil and capillary suction develops in the pore fluid; the effective stress increases and the soil undergoes vertical one dimensional settlement that is equal to the amount of water that evaporates. (d) The increased stiffness of the soil skeleton hinders further consolidation, and the membrane invades the largest pores. (e) Particles displace normal to and away from the air-water interface; pore size increases at the tip of the invading front so that

further membrane invasion is favored at the tip signaling crack initiation.

It is important to highlight that the *effective stress remains in compression everywhere in the soil mass including at the tip of the desiccation crack*.

Initiation – Surface Features

Topographic features and indentations are nucleation sites for desiccation cracks (see also Towner 1988, Zabat et al. 1997, Weinberger 1999). Furthermore, we notice in all our experiments that cracks always start at the bottom of the defect, not at the equator. Let's consider a Gaussian-shaped surface defect in a modified cam clay medium subjected to internal suction. The initial equilibrium condition is at p'=0.01 kPa with homogeneous void ratio e=3.92; suction is increased gradually to reach p'=100 kPa (Fig. 5). The far field sediment experiences 1D consolidation and reaches a void ratio e=2.105. However, the e-σ′ path at the tip gradually deviates from the e-σ′ path in the far field, and the void ratio converges to a value higher than anywhere else, i.e., allowing for preferential membrane invasion and crack initiation.

The air entry suction can be estimated from Laplace's equation in terms of pore size d_p or more conveniently in terms of specific surface S_s and void ratio e,

$$u_c^{AE} = \frac{2\,T_s}{d_p} = \frac{\rho\,T_s\,S_s}{e} \qquad (5)$$

where ρ [g/cm^3] is the mass density of the mineral that makes the particles and T_s = 0.072 N/m is the surface tension of water.

Implications

Fracture initiation and propagation based on the invasion of the water-air interfacial membrane can properly explain all known observations related to desiccation crack formation in soils, including (details in Shin and Santamarina 2009b): pore fluid and fabric effects on desiccation crack pattern (due to pore size distribution and air entry); slower crack propagation velocity as the crack approaches the free boundary of a pre-existing crack (due to delayed water migration and a smaller reduction in air-entry value next to the free boundary); right angle junction in crack pattern formation (caused by the rotation of the void ratio expansion contours towards the pre-existing free boundary); and frictional resistance responsible for the apparent tensile strength, yet with failure surface normal to the tensile direction (due to the increase in void ratio and membrane invasion normal to the applied extension).

4. Hydraulic fracture in granular materials

Hydraulic fractures affect a wide range of geosystems, and environmental applications (Massarsch 1978, Andersen et al. 1994, Garagash 2006, Soga et al. 2006). However, a proper understanding is still lacking, in part due to puzzling observations: on one hand, cohesionless-frictional sediments have no tensile strength so the failure mechanism must be different from the tension-dominated hydraulic fracture in brittle solids (Bohloli and de Pater 2006); on the other hand, hydraulic fractures in soils are in opening mode and perpendicular to the minor effective principal stress (e.g. X-ray images in Toshikazu et al. 2002), rather than Coulomb shear planes in the 45° orientation.

In this section we develop a new fundamental understanding of hydraulic fractures in granular materials that is compatible with the effective stress dependent frictional behavior of granular materials.

Invading and Host Fluids – Particle-Level Forces

Particle-level mechanisms in fluid-driven fractures depend on the miscibility between the invading fluid and the host fluid that saturates the granular medium. Relevant particle level forces in a medium made of grains size d are: skeletal force $F_{sk}=\sigma' d^2$ (associated to effective stress σ'), capillary force $F_c=\pi d T_s$ (when fluids are immis-

cible), and seepage force $F_s=3\pi\mu vd$ (when the invading fluid of viscosity μ traverses the pore space with flow velocity v). An opening will form in the soil mass when capillary and/or seepage forces exceed the skeletal force.

Fracture Initiation and Propagation

The developing of an opening driven by the forced invasion of an immiscible fluid in a soil mass resembles the formation of desiccation cracks: the interfacial membrane invades the sediment at large voids, wedge action causes the increase in pore size and allows for further membrane invasion (Fig. 6a). Numerical simulations confirm these observations (effective stress formulation, modified cam clay model, frictional media without cohesion). Similar to results obtained for the case of desiccation cracks, void ratio changes follow the 1D normal consolidation line in the far field; however, the void ratio at the tip of defects evolves to a value higher than anywhere else creating the proper situation for positive feedback that leads to crack initiation and propagation.

When miscible fluids are involved, the seepage force associated to the pore flow velocity (i.e., the imposed hydraulic gradient) generates the grain forces (i.e., effective stress field) that drive opening mode fracture propagation (Fig. 6b). In this case, the positive-feedback condition at the tip of the fracture involves: pore size opening, decreased energy loss (e.g. Hagen–Poiseuille), increase in fluid

pressure, increase in seepage force and further pore opening leading to fracture propagation orthogonal to the acting seepage force.
Hydraulic wedging in both cases, i.e., with or without an interfacial membrane, is facilitated by the initial pore size distribution near the injection point.

Experimental Evidence

The initiation of hydraulic fractures on planar surfaces is experimentally studied using a high pressure oedometric cell. A Ca-montmorillonite slurry (LL=97%; PL=47%; initial water content w=150%) is placed inside a cylindrical, stainless steel oedometer chamber and allowed to consolidate to 2 kPa. Either a miscible (water) or an immiscible fluid (oil) is placed on top of the sediment and the see-through top cap is assembled. Finally, the upper fluid is pressurized while allowing drainage through the bottom port. The soil surface is photographed using a digital camera operating in time-lapse mode. Images in Fig. 7 show the evolution of hydraulic fractures in both cases. Once again, surface defects play a critical role in fracture initiation. While drainage starts immediately after opening the bottom drainage port, there is a time delay for fracture initiation: fluid-driven separation starts when particle-level forces around surface pores or defects prompt grain separation and “hydraulic wedging”. Hence, hydraulic fracturing is intimately linked to pressure diffusion.

Discussion on Pore Size Distribution

Pore size distribution plays a prevalent role on fracture initiation pressure in fluid driven cracks as large pores tend to be invaded/enlarged first. Sediments typically exhibit a log-normal pore size distribution rather than uniform distribution (Garcia-Bengochea, et al., 1979; Juang and Holtz, 1986; Tanaka, et al., 2003), and the standard deviation σ^* in logarithmic scale $\log(d_p/1\mu m)$ is between $0.3 \leq \sigma^* \leq 0.7$. Fracture initiation starts at large pores that are α-standard deviations above the mean pore size $\bar{d}$; this is the characteristic pore size $d_p^* = \bar{d} \cdot 10^{\alpha\sigma^*}$.

This result can be used to obtain a lower estimate of the capillary pressure at fracture initiation and to obtain the spacing at fracture saturation (see details in Shin 2009). It can be concluded that the pressure at fracture initiation will be lower in soils with wider pore size distributions, at the same global void ratio.

5. Conclusions

Discontinuous planes often develop in soils. These discontinuities affect the mechanical behavior (stiffness and strength) and transport properties of sediments (fluid migration and diffusion). The fundamental understanding of the development of discontinuities in soils

must be compatible with their inherent granular nature and effective-stress dependent behavior.

Dissolution is an ubiquitous phenomenon in soil diagenesis. Particle-level volume reduction in uncemented granular media under zero-lateral strain boundary conditions causes a decrease in horizontal stress, leading to internal shear failure conditions and the potential development of shear strain localization. Both the genesis of polygonal fault systems and the magnitude of shear displacements they experienced can be properly explained assuming mineral dissolution during sediment diagenesis.

While dry or drained granular materials fail in shear only (in agreement with the Coulomb criterion), saturated granular materials can couple granular behavior with fluid flow to give rise to opening type failure modes where the fracture walls are kept open by the interaction between the invading fluid and the granular medium.

Skeletal forces (effective stress dependent), capillary forces (when immiscible fluids are involved) and seepage drag-forces (associated with flow velocity) interact at surface defects or large surface pores to give rise to positive feedback mechanisms that promote fracture initiation and propagation: particle displacement around the largest pores enlarge voids at the tip to facilitate further localized invasion.

Desiccation cracks are an example of localized invasion of the interfacial membrane between water and air.

Effective stresses remain in compression everywhere throughout the granular medium including at the tip of opening fractures.

Acknowledgments: Support for this research was provided by the Goizueta Foundation and the National Science Foundation. These studies evolved from interactions with J. Cartwrigth (polygonal faults), M. Dusseault and L. Germanovich (hydraulic fracture), and Salvador Lazcano (desiccation cracks).

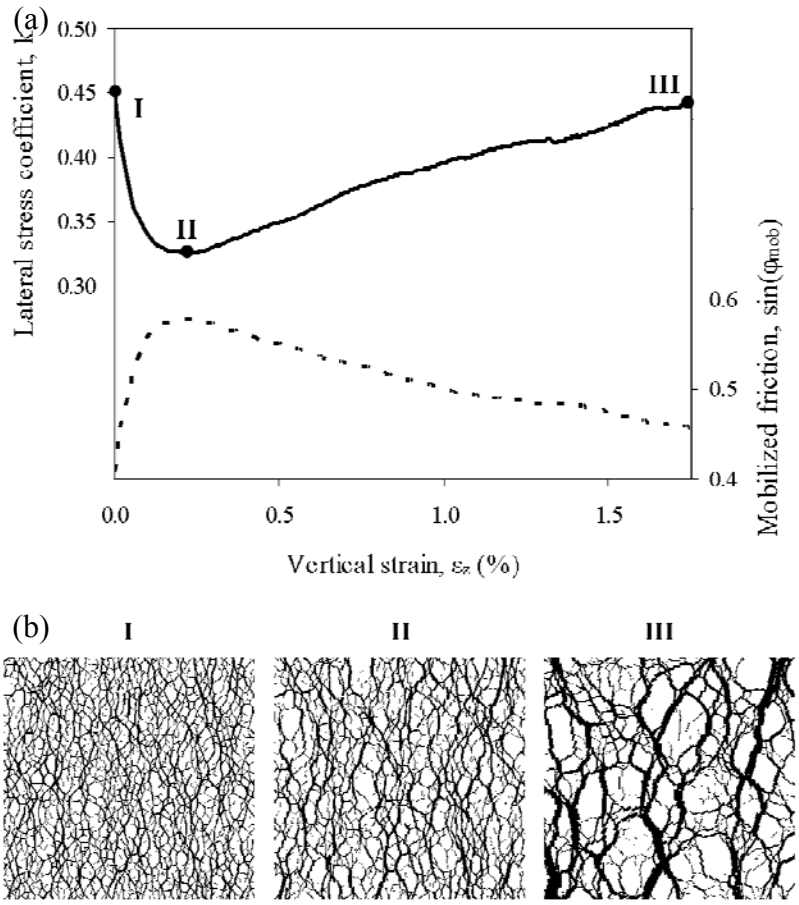

Fig. 1. Sediment evolution during particle dissolution. Discrete element simulation of a 2D packing of 9999 disks. The diameter of 20% of the particles - selected at random- is gradually reduced while keeping zero lateral strain and constant vertical stress boundary conditions. (a) Lateral stress coefficient k and mobilized friction, (b) Interparticle force networks at different stages of dissolution.

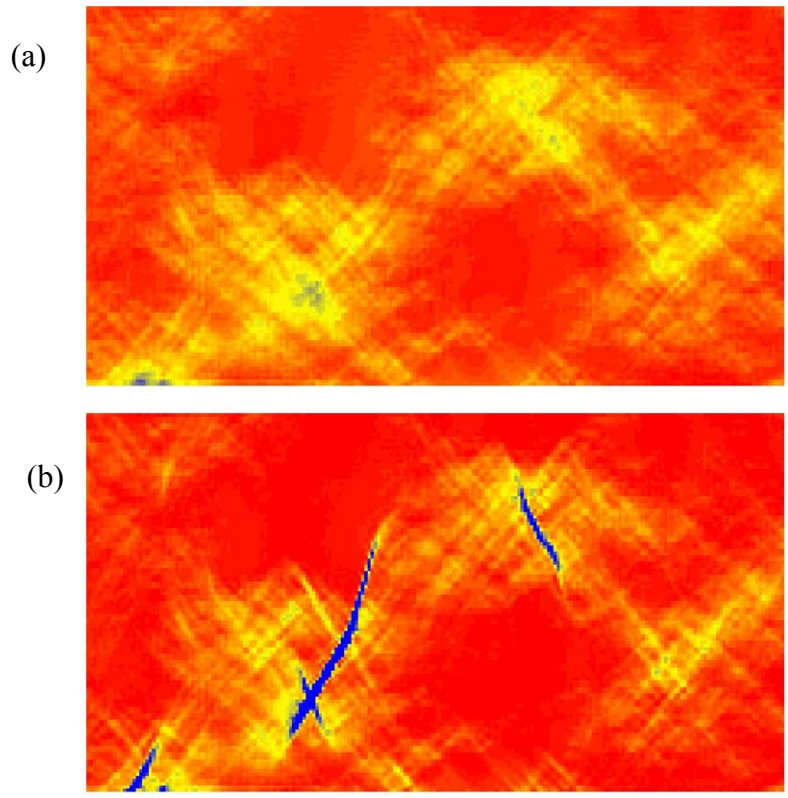

Fig. 2. Finite element simulation - Correlated random field of volume contraction within a frictional material. (a) Diffused deviatoric strain distribution in perfectly plastic medium – without softening $\phi_{res}=\phi_p= 30°$. (b) Shear strain localization is facilitated if there is post peak strain softening ($\phi_p= 30°$, $\phi_{res}= 10°$).

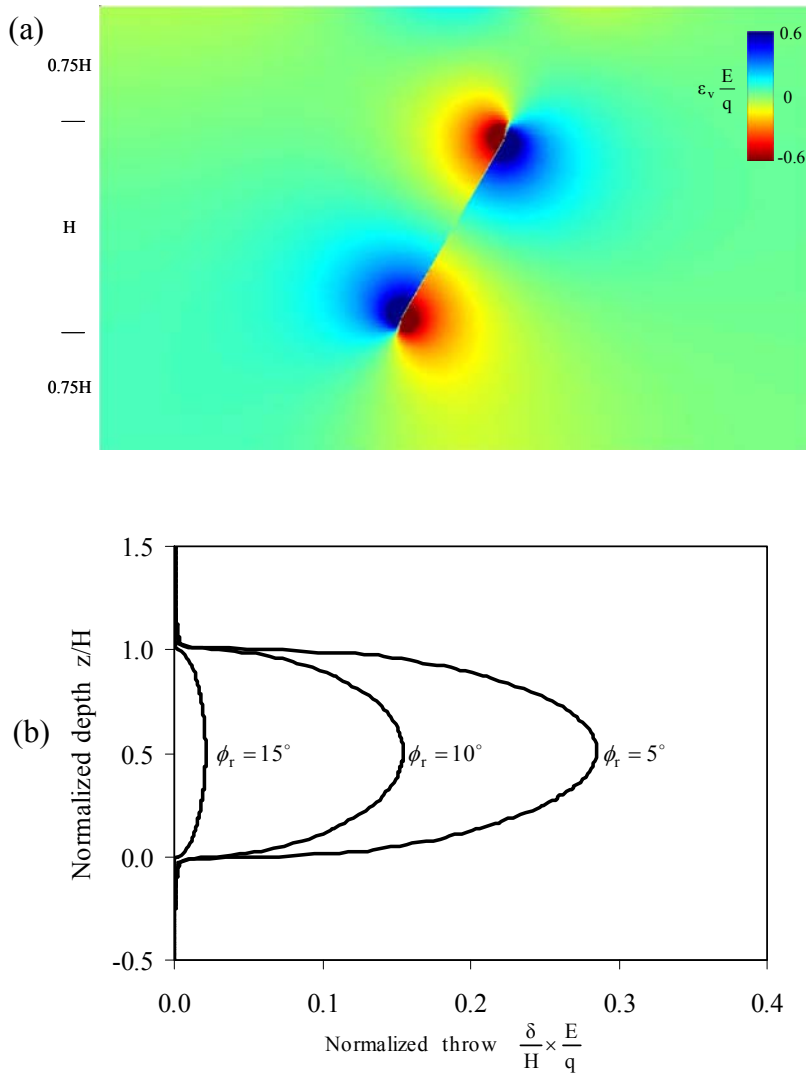

Fig. 3. Strain and displacement field after fault slippage for a medium with constant stiffness with depth. (a) Normalized volumetric strain $\varepsilon_v E/q$ (Contractive is positive - blue). (b) Normalized throw along the fault length for different residual friction angles. Model parameters: sediment friction angles $\phi=30°$, $\phi_{res}=5°$, initial state of stress $k_0=1-\sin\phi=0.5$, fracture orientation $\beta=45°+\phi/2=60°$.

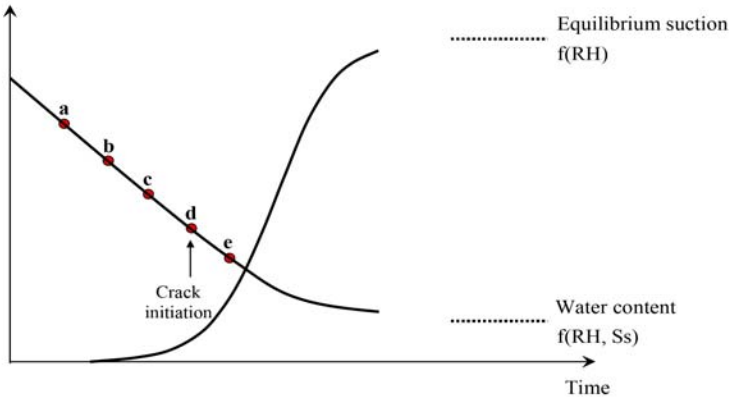

Stages	a	b	c	d	e
Global view	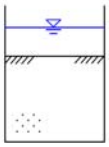	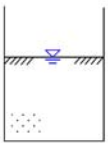	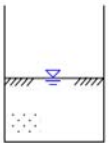	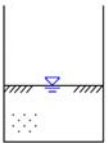	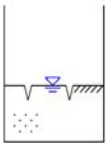
Particle scale view	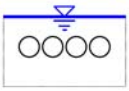	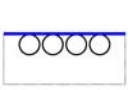	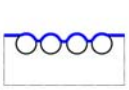	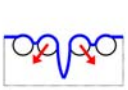	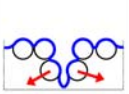
Comments	Evaporation of supernatant water No suction No strain in the soil skeleton	Air-water interface membrane reaches the soil surface	Membrane forms around soil particles Suction increases Consolidation of soil skeleton and increase in stiffness	Air invades the largest pores The air-water interface membrane pushes particles away from the invaded pore. Pore size increase at the tip and crack grows	Crack propagation and formation of polygons Vertical deformation ceases Eventually, the soil mass becomes unsaturated

Fig. 4. Water evaporation, soil desiccation and crack formation - Summary of pore and particle scale processes.

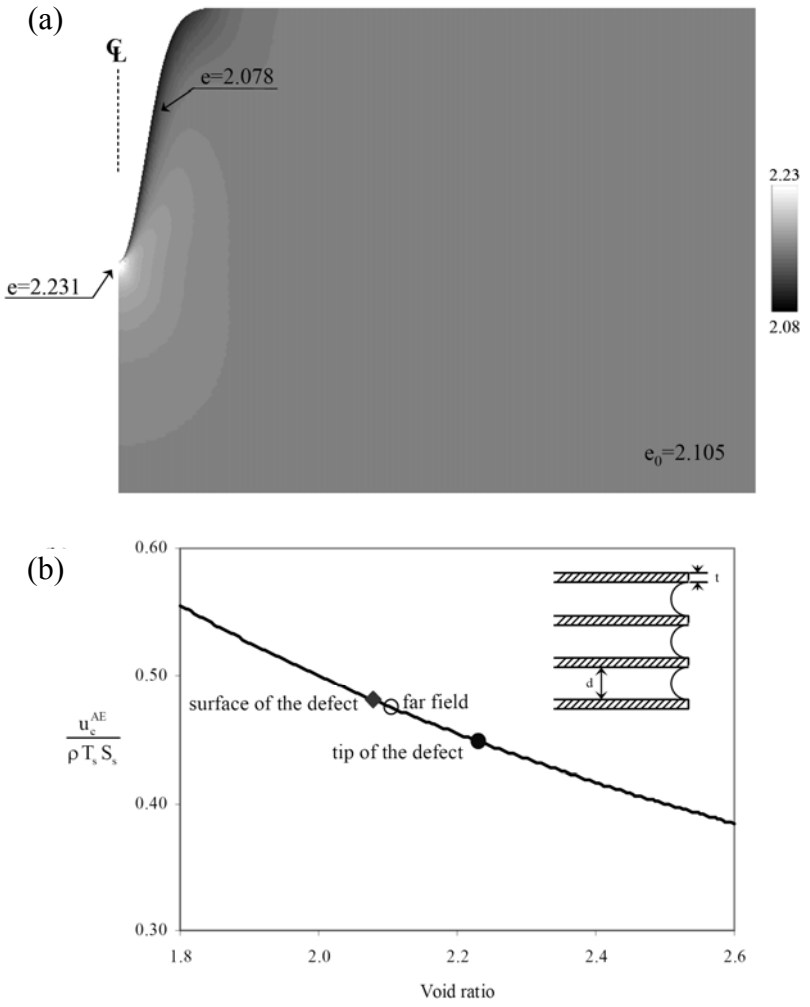

Fig. 5. Surface defects and crack initiation. Local void ratio evolution during desiccation - Finite element analysis. The domain size is 6mm×6mm, and the defect depth is 1mm. (a) Void ratio when suction u=100kPa. (b) Required suction for air entry at the tip and on the surface as a function of the local void ratios.

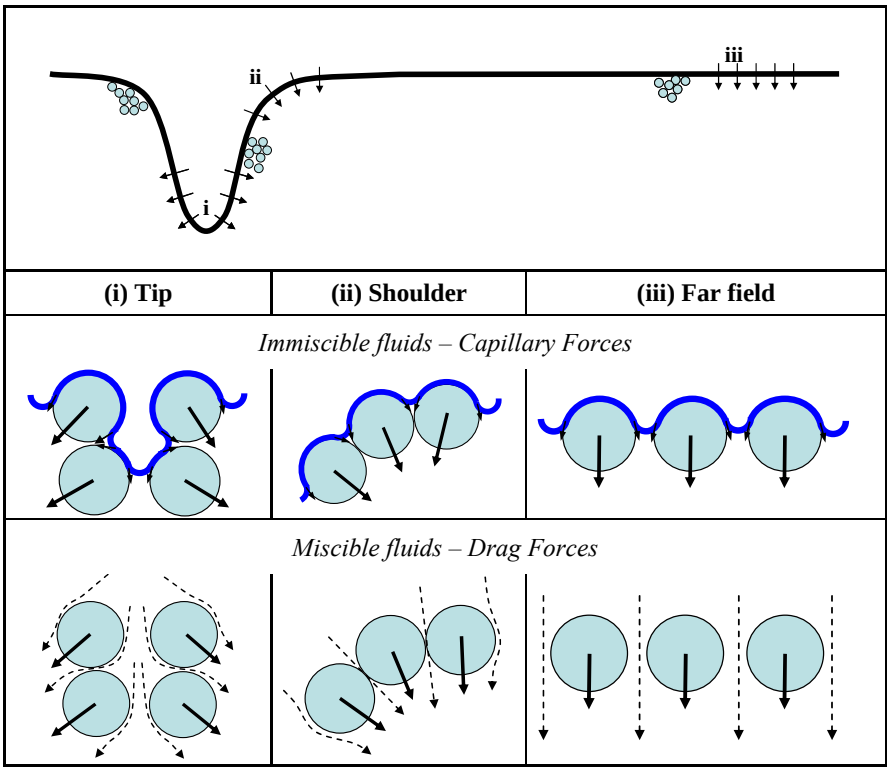

Fig. 6. Void ratio evolution around a surface defect during the forced invasion of (a) an immiscible fluid, and (b) a miscible fluid.

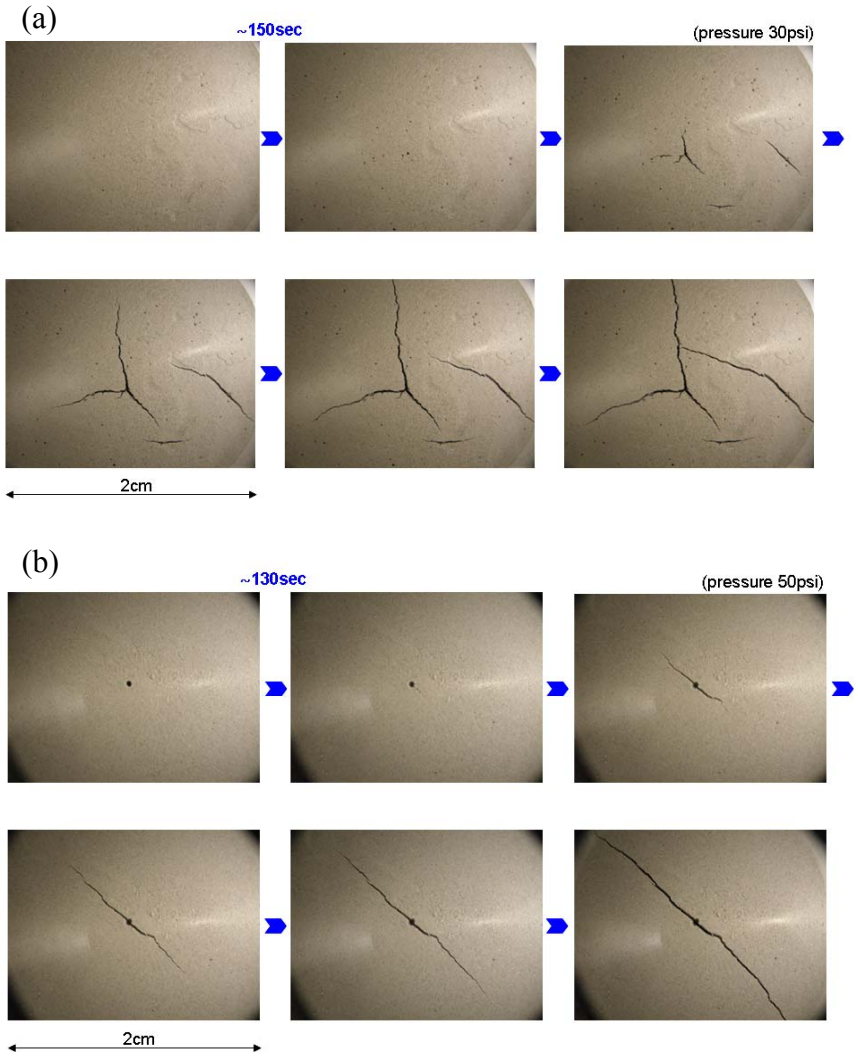

Fig. 7. Hydraulic fracture formation on the soil surface. (a) Immiscible fluid. (b) Miscible fluid.

References

Andersen KH, Rawlings CG, Lunne TA et al (1994) Estimation of hydraulic fracture pressure in clay. Canadian geotechnical journal 31:817-828

Barnett JAM, Mortimer J, Rippon JH et al (1987) Displacement geometry in the volume containing a single normal fault. American Association of Petroleum Geologists Bulletin 71:925-937

Bohloli B, de Pater CJ (2006) Experimental study on hydraulic fracturing of soft rocks: Influence of fluid rheology and confining stress. Journal of Petroleum Science and Engineering 53:1-12

Burland JB (1990) On the compressibility and shear-strength of natural clays. Geotechnique 40:329-378

Cartwright JA, Dewhurst DN (1998) Layer-bound compaction faults in fine-grained sediments. Bulletin of the Geological Society of America 110:1242-1257

Cowie PA, Scholz CH (1992) Physical explanation for the displacement length relationship of faults using a post-yield fracture-mechanics model. Journal of Structural Geology 14:1133-1148

Desrues J, Viggiani G (2004) Strain localization in sand: an overview of the experimental results obtained in Grenoble using stereophotogrammetry. International Journal for Numerical and Analytical Methods in Geomechanics 28:279-321

Garagash DI (2006) Propagation of a plane-strain hydraulic fracture with a fluid lag: Early-time solution. International Journal of Solids and Structures 43:5811-5835

Garcia-Bengochea I, Lovell CW, Altschaeffl AG (1979) Pore distribution and permeability of silty clays. Journal of the Geotechnical Engineering Division 105:839-856

Jaky J (1944) The coefficient of earth pressure at rest. Journal of the Union of Hungarian Engineers and Architects 355-358.

Juang CH, Holtz RD (1986) Fabric pore size distribution, and permeability of sandy soils. Journal of geotechnical engineering ASCE 112:855-868

Lachenbruch AH (1962) Mechanics of thermal contraction cracks and ice-wedge polygons in permafrost. Geological Society of America, New York

Lade PV (2002) Instability, shear banding, and failure in granular materials. International Journal of Solids and Structures 39:3337-57

Massarsch KR (1978) New aspects of soil fracturing in clay. Journal of the Geotechnical Engineering Division ASCE 104:1109-1123

Perrin G, Leblond JB (1993) Rudnicki and Rice analysis of strain localization revisited. Journal of Applied Mechanics-Transactions of the ASME 60:842-846

Rudnicki JW, Rice JR (1975) Conditions for the localization of deformation in pressure-sensitive dilatant materials. Journal of the Mechanics and Physics of Solids 23:371-394

Santamarina JC, Klein KA, Fam MA (2001) Soils and waves : particulate materials behavior, characterization and process monitoring, J. Wiley & Sons, New York

Schultz RA, Okubo CH, Wilkins SJ (2006) Displacement-length scaling relations for faults on the terrestrial planets. Journal of Structural Geology 28:2182-2193

Shin H (2009) Development of discontinuities in granular media. Georgia Institute of Technology, Atlanta

Shin H, Santamarina JC (2009a) Mineral dissolution on ko effects Journal of Geotechnical and Geoenvironmental Engineering ASCE in press

Shin H, Santamarina JC (2009b) Desiccation cracks in saturated fine-grained soils: Particle level phenomena and effective stress analysis under review

Shin H, Santamarina JC, Cartwright JA (2008) Contraction-driven shear failure in compacting uncemented sediments. Geology 36:931-934

Shin H, Santamarina JC, Cartwright JA (2009) Displacement field in contraction driven faults under review

Soga K, Gafar KO, Ng MYA et al (2006) Macro and micro behaviour of soil fracturing. International Symposium on Geomechanics and Geotechnics of Particulate Media - Geomechanics and Geotechnics of Particulate Media, Yamaguchi Japan 421-427

Tanaka H, Shiwakoti DR, Omukai N et al (2003) Pore size distribution of clayey soils measured by mercury intrusion porosimetry and its relation to hydraulic conductivity. Soils and Foundations 43:63-73

Toshikazu H, Yoshiyuki M, Kenichi M et al (2002) Features of crack propagation by hydraulic fracturing in cohesive soil. Experimental study on seepage failure of small earth dams. Transactions of the Japanese Society of Irrigation, Drainage and Reclamation Engineering 219:383-392

Towner GD (1988) The influence of sand- and silt-size particles on the cracking during drying of small clay-dominated aggregates. Journal of Soil Science 39:347-356

Vermeer PA (1990) The orientation of shear bands in biaxial tests. Geotechnique 40:223-236

Weinberger R (1999) Initiation and growth of cracks during desiccation of stratified muddy sediments. Journal of Structural Geology 21:379-386

Zabat M, Vayer-Besançon M, Harba R et al (1997) Surface topography and mechanical properties of smectite films, Springer, Berlin